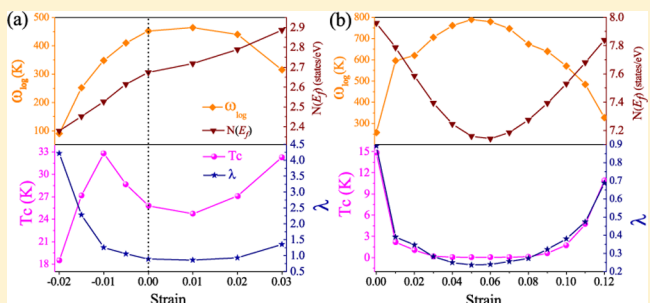


Strain Effect on the Superconductivity in Borophenes

Geng Li,^{†,‡} Yinchang Zhao,[§] Shuming Zeng,[†] M. Zulfiqar,^{†,‡} and Jun Ni^{*,†,‡,§}[†]State Key Laboratory of Low-Dimensional Quantum Physics, Department of Physics, Tsinghua University, Beijing 100084, People's Republic of China[‡]Collaborative Innovation Center of Quantum Matter, Beijing 100084, People's Republic of China[§]Department of Physics, Yantai University, Yantai 264005, People's Republic of China

ABSTRACT: The effects of strain on the structure stability, electron–phonon coupling (EPC), and superconductivity of two types of monolayer borophenes realized in the experiments are systematically investigated within the framework of density functional theory. We find that the electron–phonon coupling (EPC) in the buckled triangle borophene can be significantly enhanced by the suitable strain (−2–3%) due to the lower acoustic phonon branch softening. Our calculations suggest that a superconducting transition temperature (T_c) ranging from 24 to 32 K may be observed in the experiment. For the β_{12} borophene, the EPC constant (λ) and T_c exhibit a U-curve variation with the strain ranging from 0 to 12%. The highest T_c of 14.9 K can be obtained in the pristine structure. The stiffness of the lower acoustic phonon branches and the U-curve variation of $N(E_F)$ mainly from the p_z electrons of boron are responsible for the change of the superconducting transition temperature with the increase of the tensile strain. Although borophenes have a highly anisotropic structure, the uniaxial strain effect on the superconductivity is isotropic.



INTRODUCTION

Within the knowledge of the Bardeen–Cooper–Schrieffer (BCS) theory,¹ the superconducting transition temperature is positively related to the phonon vibration frequency that is inversely proportional to the square root of the atomic mass. It provides a practical principle: the superconductivity with the higher T_c may exist in the materials composed of the lighter atoms. Under the guide of this principle, surprising progress has been made in the conventional superconductivity. The metallic hydrogen has been predicted to have a very high T_c of about 100–240 K for molecular hydrogen² and 300–350 K for the atomic phase at 500 GPa.³ Theoretical and experimental studies in parallel report that sulfur hydrides exhibit a $T_c \sim 200$ K under high pressures.^{4–6} The metallic face-centered cubic lithium possesses a $T_c \approx 70$ K at 40 GPa.^{7,8}

Like hydrogen, boron is also a light-mass element, which originally induces the high- T_c superconductivity, such as MgB₂.^{9–11} However, in the pure bulk boron under ambient pressure without any doping, there is no evidence of superconductivity.¹² Recently, borophenes, several boron sheets consisting of the fifth element boron in the periodic table, have been grown epitaxially on the Ag(111) substrate under ultrahigh-vacuum conditions by different groups.^{13,14} Theoretical calculations predicted numerous freestanding borophenes, whose structures consist of triangular boron grid with different densities of the hexagonal hole.^{15–20} Because of the interfacial interactions of Ag substrate and effect of the temperature, the scanning tunneling microscopy images revealed three structures of borophene: the buckled triangular sheet, β_{12} sheet, and χ_3 sheet. In the β_{12} sheet, there exists

massless Dirac fermions with nontrivial Berry phases.²¹ Two-dimensional (2D) materials showing superconductivity have an important application in nanoscale superconducting devices, such as superconducting quantum interference devices and superconducting transistors.^{22–24} Many theoretical calculations based on the BCS theory predicted that the 2D materials may become a good superconductor under strain modulation or carrier doping. For instance, when the doping level is $\sim 4 \times 10^{14} \text{ cm}^{-2}$ combined with the strain of $\sim 16\%$, the superconducting transition temperature above the liquid hydrogen temperature can be expected in the semimetal graphene.^{25,26} With the effects of the strains and carrier doping, the semiconducting phosphorene becomes superconductor and the T_c ranges from 3 to 16 K.²⁷ The highest superconducting transition temperature can reach to 22 K in MoS₂ monolayer under strain and doping.²⁸ In these 2D monolayers, the electron–phonon coupling (EPC) has been enhanced by the strain to some extent. Different from these semiconductors, borophenes have the inherent metallicity. Therefore, the emergence of borophenes triggered a surge of interest in the investigation of the superconductivity. Zhao et al. made a systematic study on superconductivity for two-dimensional boron allotropes, and they found a V-shape dependence of T_c on the hexagon hole density.^{8,20} Gao et al. and Penev et al. reported that the freestanding borophenes realized in experiments present a phonon-mediated superconductivity with the

Received: April 3, 2018

Revised: June 22, 2018

Published: July 3, 2018

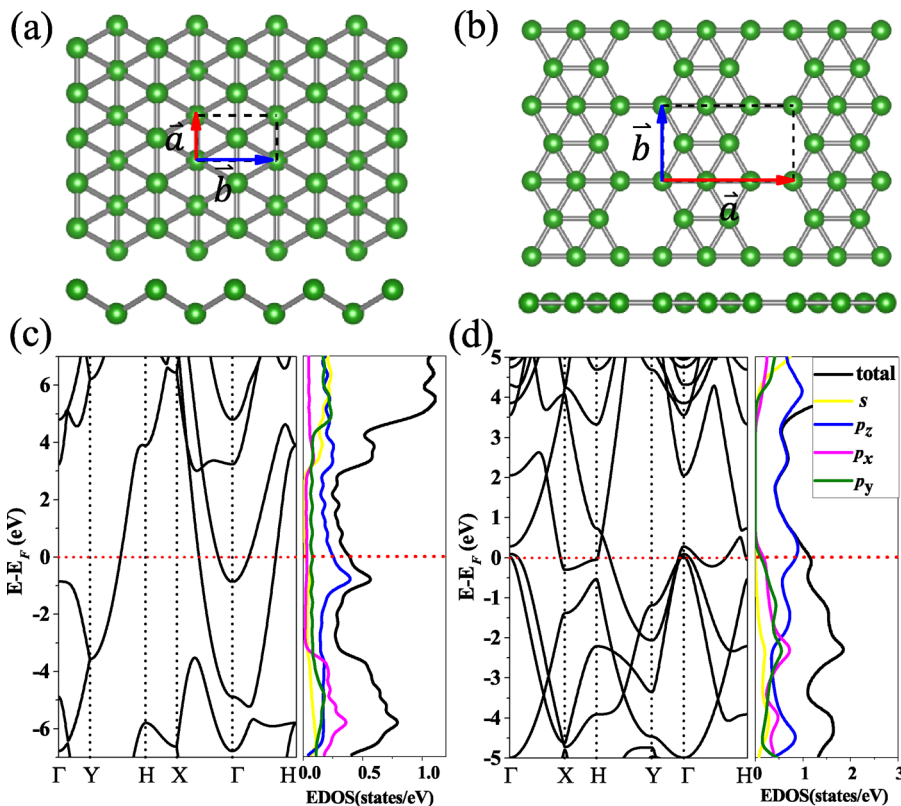


Figure 1. Electronic structures of the pristine borophene. Top and side view of the structures of (a) the buckled triangle structure and (b) β_{12} structure. Band structures and projected electron density of states (EDOS) around the Fermi level for (c) the buckled triangle structure and (d) β_{12} structure. The Fermi energy depicted with the red dashed line is set to be zero.

T_c about 20 K.^{29,30} However, to date, no systemic investigation of the strain effect on the EPC and superconducting properties in borophenes has been reported.

Two types of borophene have been chosen to investigate the superconductivity under different strains. The superconducting transition temperature is calculated to be 25.8 K for the pristine buckled triangle structure and 14.9 K for the β_{12} structure. The softening phonon frequency induced by the strain leads to the dynamic instability of their structures. In the safe area of the strain, we have discussed the strain effect on the electron density of states (EDOS) at Fermi surface (FS), logarithmically averaged phonon frequency, EPC constant, phonon dispersion spectrum, Eliashberg function, and superconducting transition temperature. We find that the strain has the different effects on the superconductivity for the two structures. Both tensile and compressive strains obviously enhance the EPC in the buckled triangle borophene, whereas the EPC of the β_{12} borophene sharply decreases and then increases. The lower-frequency acoustic phonon affected by the strain plays an important role to explain the variation of the T_c .

METHODS

All of the electronic structures and EPC properties are calculated within DFT and density functional perturbation theory,³¹ implemented in the QUANTUM-ESPRESSO package.³² The ultrasoft pseudopotential with a cutoff energy of 55 Ry is adopted to describe the interaction between electrons and ionic cores, which has been proved to be sufficient for convergence of the EPC parameter in ref 15. The generalized gradient approximation of PW91³³ is employed for the

exchange–correlation energy functional. Our borophene models contain a vacuum space of 20 Å in the c axis to avoid the interactions between the adjacent images. By changing the lattice constants, we add the biaxial strains to the borophenes. The in-plane strength is defined as $\epsilon = (a - a_0)/a_0 \times 100\%$, where a and a_0 are the in-plane lattice constants of the strained and unstrained monolayer borophenes, respectively. All of the structures are fully relaxed until the force convergence criteria is less than 10^{-5} Ry/b.

For the buckled triangle borophene, we use a k -mesh of $40 \times 40 \times 1$ and a q -mesh of $10 \times 10 \times 1$ to calculate the dynamical matrices and electron–phonon matrix. After the convergence testing in β_{12} borophene, the Brillouin zone for the self-consistent electron calculations is sampled in a $24 \times 40 \times 1$ k -points grids with a Methfessel–Paxton smearing of 0.02 Ry and the phonon and superconducting properties are calculated on a $6 \times 12 \times 1$ q -point mesh.

The Eliashberg approach^{34–36} has succeeded in estimating the EPC of borophene in previous work.^{8,20,29,37} By solving the phonon dispersion and the EPC matrix, the Eliashberg spectral function $\alpha^2 F(\omega)$ has the following formula

$$\alpha^2 F(\omega) = \frac{1}{2\pi N(E_F)} \sum_{\mathbf{q}\nu} \delta(\omega - \omega_{\mathbf{q}\nu}) \frac{\gamma_{\mathbf{q}\nu}}{\hbar\omega_{\mathbf{q}\nu}} \quad (1)$$

with

$$\begin{aligned} \gamma_{\mathbf{q}\nu} = & 2\pi\omega_{\mathbf{q}\nu} \sum_{i,j} \int \frac{d^3k}{\Omega_{BZ}} |g_{\mathbf{q}\nu}(\mathbf{k}, i, j)|^2 \delta(e_{\mathbf{q},i} - e_F) \\ & \times \delta(e_{\mathbf{k}+\mathbf{q},i} - e_F) \end{aligned} \quad (2)$$

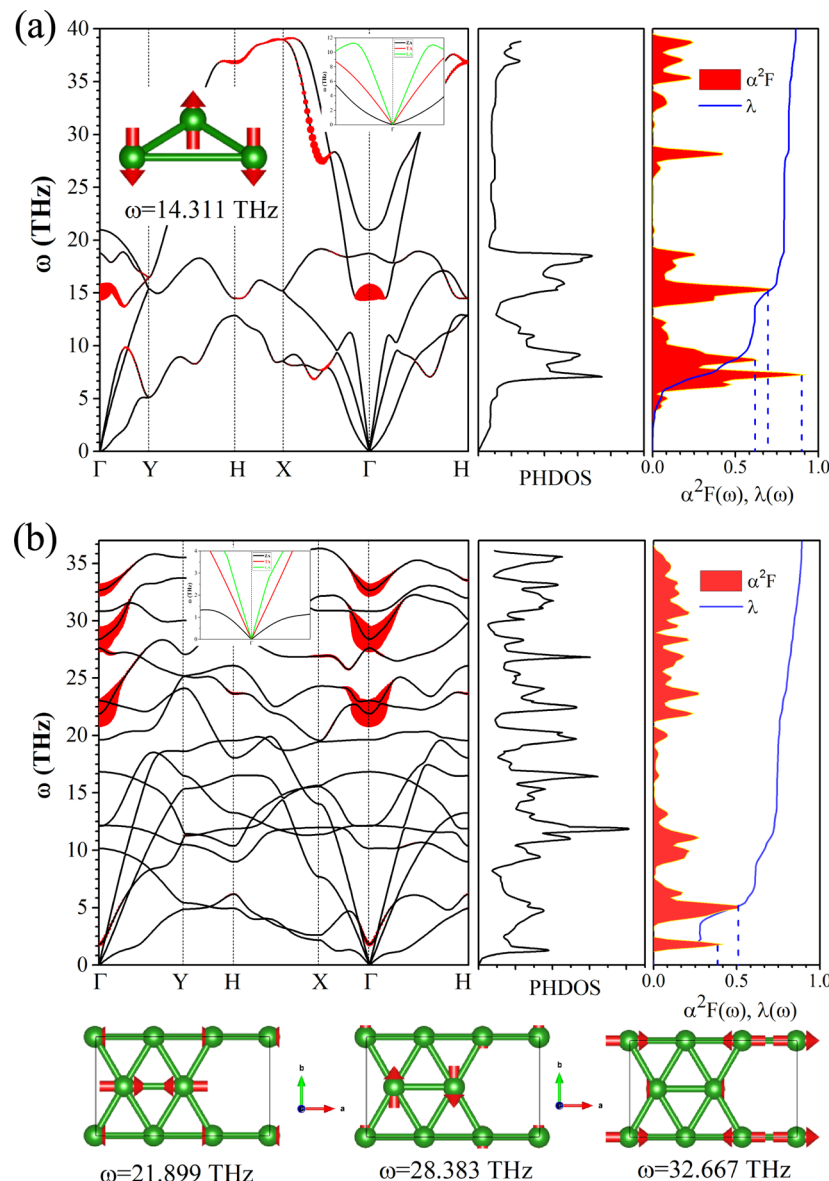


Figure 2. Phonon dispersion with phonon line width $\gamma_{\mathbf{q}\nu}$, phonon density of states (PDOS), Eliashberg function $\alpha^2F(\omega)$ and EPC constant $\lambda(\omega)$, and phonon vibration modes at the Γ point for the (a) buckled triangle structure and (b) β_{12} structure. The red arrows and their lengths represent the directions and relative amplitudes of these vibrational modes, respectively. The enlarged view of the acoustic phonon modes around the Γ point is plotted in the inset for the buckled triangle structure and β_{12} structure.

$\alpha^2F(\omega)$ is related to three physical quantities: phonon frequency ($\omega_{\mathbf{q}\nu}$), the electronic density of states at the Fermi level ($N(E_F)$), and the line width of phonon mode ν at the wave vector \mathbf{q} ($\gamma_{\mathbf{q}\nu}$). $\gamma_{\mathbf{q}\nu}$ depends on the volume of the BZ (Ω_{BZ}) and the EPC matrix element ($g_{\mathbf{q}\nu}(\mathbf{k}, i, j)$). All of the Dirac δ functions in the equations are simulated with the Gaussian functions. Through the frequency-space integration for the Eliashberg spectral function, the total EPC constant λ and the logarithmically averaged phonon frequency ω_{\log} can be obtained

$$\lambda = 2 \int_0^\infty \alpha^2F(\omega) \frac{d\omega}{\omega} \approx \frac{1}{N_{\mathbf{q}}} \sum_{\mathbf{q}\nu} \lambda_{\mathbf{q}\nu} \quad (3)$$

$$\langle \omega_{\log} \rangle = \exp \left(\frac{2}{\lambda} \int_0^\infty \alpha^2F(\omega) \log \frac{d\omega}{\omega} \right) \quad (4)$$

Finally, we get the Allen–Dynes-modified McMillan equation to estimate the T_c as follows

$$T_c = \frac{\langle \omega_{\log} \rangle}{1.2} \exp \left(-\frac{1.04(1 + \lambda)}{\lambda - \mu^*(1 + 0.62\lambda)} \right) \quad (5)$$

where μ^* is the retarded Coulomb pseudopotential with the reasonable value of 0.13.^{38–40}

RESULTS AND DISCUSSION

Considering the structural inconvenience of adding the biaxial strain on the χ_3 structure, our calculations just consider the buckled triangle borophene and β_{12} , in which a rectangular lattice has been adopted. As revealed by the experiment,¹³ the buckled triangle borophene with symmetry belonging to the $Pmmn$ symmetric group has a highly anisotropic structure with the pucker in the b direction. The fully optimized lattice parameters are $a = 1.618$ Å and $b = 2.873$ Å, which are smaller

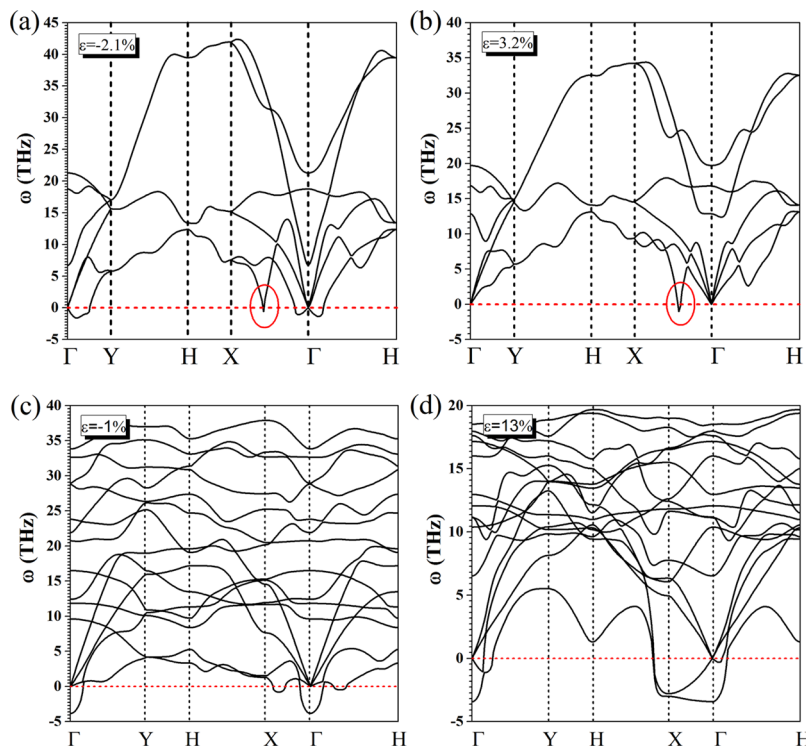


Figure 3. Phonon dispersion spectra at critical strains: for the buckled triangle borophene under the strain of (a) $\epsilon = -2.1\%$ and (b) $\epsilon = 3\%$ and for the β_{12} borophene at (c) $\epsilon = -1\%$ and (d) $\epsilon = 12\%$.

than those of the experiment,¹³ but consistent with the previous theoretical values,³⁷ as shown in Figure 1a. The corresponding band structures and EDOS are presented in Figure 1c, which indicates that its pristine structure is metallic and the DOS in FS $N(E_F)$ is 0.40 states/eV per unit cell, coming mostly from the p_z orbitals.

Figure 1b shows the structure of β_{12} borophene with the symmetry $Pmmm$. After structural optimization, the lattice constants along the a and b axes are 5.065 and 2.923 Å, respectively, coinciding with previous results.²⁹ The calculated band structures and projected EDOS are given in Figure 1d. The states at FS are mostly occupied with the p_z electrons with the $N(E_F) \sim 1.15$ states/(eV cell). When the strain is applied on the borophene, the p_z electrons make the primary contributions to the EPC.

First, we calculate the possible superconductivity of the pristine borophene. The phonon dispersion with phonon line width γ_{qv} , phonon density of states, and Eliashberg spectral functions $\alpha^2F(\omega)$ and $\lambda(\omega)$ for the buckled triangle borophene and β_{12} borophene with no strain are shown in Figure 2a,b. Our calculated phonon spectra for the buckled triangle borophene and β_{12} borophene are consistent with reported works.^{20,29,30} The enlarged view of the acoustic phonon modes around the Γ point is linear or parabolic, as plotted in the inset of Figure 2a,b, agreeing well with the case in the graphene and silicene.^{26,41} There is no imaginary phonon mode in the phonon dispersion, which shows that the pristine borophenes are dynamically stable. Figure 2a shows that larger than 70% of phonon line width γ_{qv} arises from the phonon frequency ~ 15 THz around the Γ point, which is from the relative out-of-plane vibration between boron atoms. In the Eliashberg spectral function, there is also a peak around $\omega \sim 15$ THz. But its contribution to the EPC constant λ is less than 20%. This is because the $\alpha^2F(\omega)$ is the function of γ_{qv}/ω_{qv} (eq 1) and $\lambda(\omega)$

contains $\alpha^2F(\omega)/\omega$ (eq 3). Actually, we find that the low-frequency (5–12 THz) acoustic phonon leads to the largest contribution to the EPC. They account for 69.53% of the total λ . As a result, our calculated $\lambda = 0.87$ and $\omega_{log} = 452.67$ K result in a $T_c = 25.81$ K for the buckled triangle borophene.

Figure 2b shows the calculated superconductivity of the pristine β_{12} borophene. The γ_{qv} mainly locates in the three high phonon frequencies (21.90, 28.38, and 32.67 THz) around the Γ point, which are caused by the relative in-plane vibration of the different neighboring pairs of borons. As the same reason above, the phonon modes in the corresponding frequencies have a contribution less than 15% to the total λ . The primary part (about 68.31%) of the total λ comes from the low-frequency (0–8 THz) acoustic modes around the Γ point. Finally, we obtain the $T_c = 14.84$ K of the β_{12} borophene with $\lambda = 0.90$ and $\omega_{log} = 257.13$ K.

When borophenes are grown on the substrate, the strain effect on the electronic and superconducting properties has been introduced. Therefore, we add the strain by changing the lattice parameters to simulate the borophenes grown on the substrate and calculate the strain effect on the Coulomb interaction and phonon coupling on borophenes. First, we discuss the dynamical stability of the structure of borophenes under different strains. The tensile and compressive strains have been applied on the two structures (positive value for tensile train and negative value for compressive strain). The corresponding phonon spectra at the critical strains are calculated by the quasi-harmonic approximation, as shown in Figure 3. The emergence of the imaginary frequency not around the Γ point determines the critical strains that indicate the instability of the structure. We find that the buckled triangle borophene is stable under the strain region of $-2.0\% \leq \epsilon \leq 3.1\%$, whereas for the β_{12} borophene, either compressive strain or the tensile strain beyond 12% gives rise to its

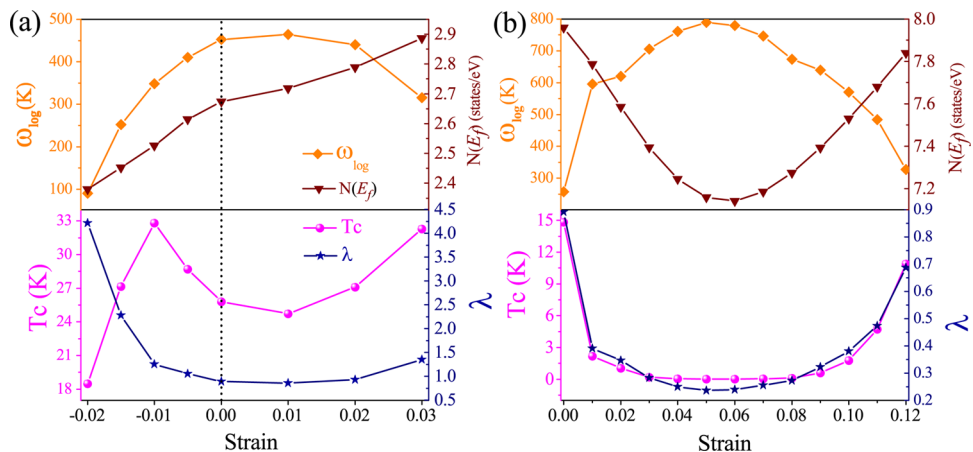


Figure 4. Superconducting transition temperature T_c (magenta), EPC constant λ (blue), DOS of the FS $N(E_F)$ (red), and logarithmically averaged phonon frequency ω_{\log} (orange) versus the strain ϵ for the (a) buckled triangle borophene and (b) β_{12} borophene, respectively.

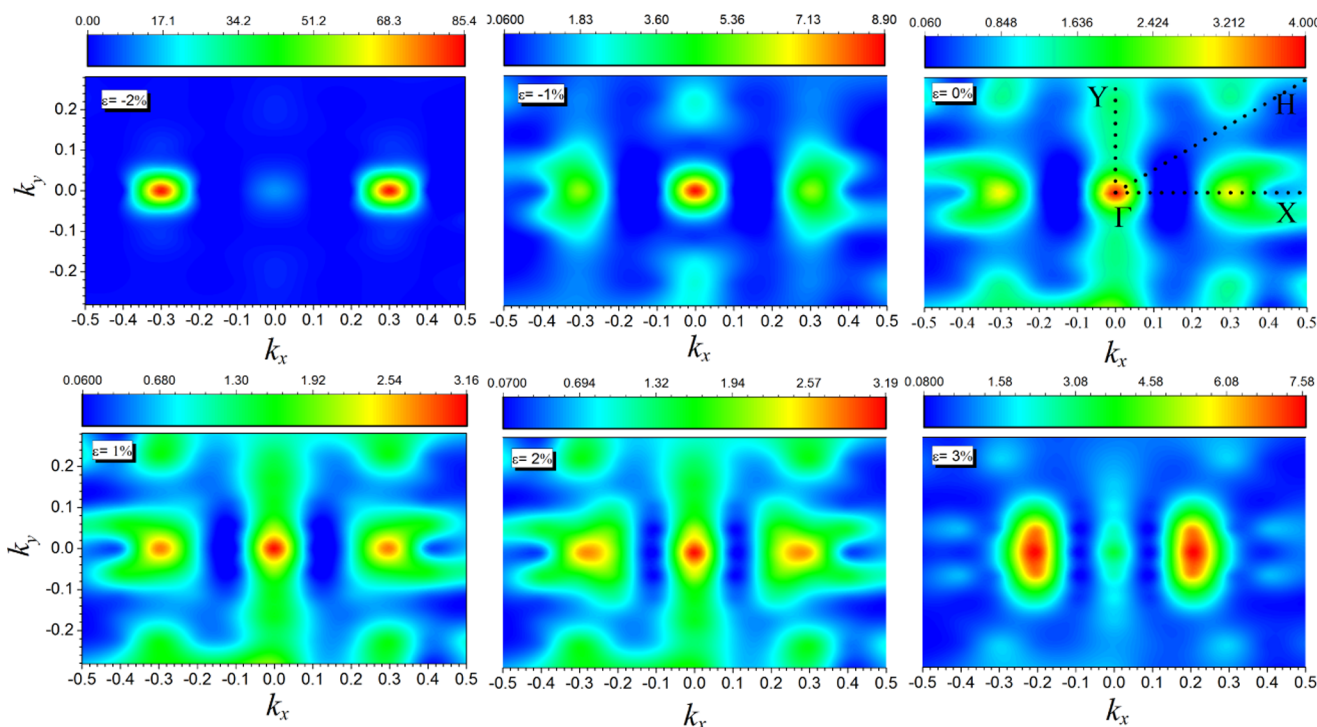


Figure 5. Distribution map of wave-vector-resolved EPC constants λ_q for the buckled triangle borophene under different biaxial strains from -2 to 3% .

instability. The phonon spectra of the buckled triangle borophene under $\epsilon = -2.1$ and -3.2% are displayed in Figure 3a,b, respectively. The instability originates from the softened phonon mode along the X point to Γ point, which plays a significant role in the superconductivity. Figure 3c,d exhibits the phonon spectrum for the β_{12} borophene with the critical strains (-1 and 13%). The acoustic phonon modes around the X point are softened by the strains. These softening phonon can be understood by the Kohn anomaly.^{26,27}

Figure 4a,b shows the strain effects on T_c , λ , $N(E_F)$, and ω_{\log} for the buckled triangle borophene and β_{12} borophene, respectively. When the strain applied on the buckled triangle borophene ranges from -2 to 3% , the DOS at FS $N(E_F)$ increases, whereas the logarithmically averaged phonon frequency ω_{\log} increases and then decreases with the maximum at $\epsilon = 1\%$. However, the EPC constant λ is contrary in the

tendency to ω_{\log} when changing ϵ . Both the tensile and compressive strains enhance the EPC. The superconducting transition temperature T_c vs ϵ shows the similar trend with λ vs ϵ except for $\epsilon = -2\%$, and a local minimum $T_c = 24.75$ K appears at $\epsilon = 1\%$, as shown in Figure 4a. Because of the small value of ω_{\log} at $\epsilon = -2\%$, T_c sharply declines to 18.5 K. The maximum T_c of about 32 K is reached at the strain of -1 or 3% . Considering the effect of the substrate on the lattice constants, the superconductivity may be realized experimentally in the metallic buckled triangle borophene with the T_c between 24 and 32 K.

For the β_{12} borophene, T_c , λ , and $N(E_F)$ share the similar U-curve variation with the strain range from 0 to 12% . The minimum value locates at $\epsilon = 6\%$. However, the variation trend of ω_{\log} vs ϵ is in contrary with that of $N(E_F)$, λ , and T_c vs ϵ (see Figure 4b). It means that with increasing strains, T_c is

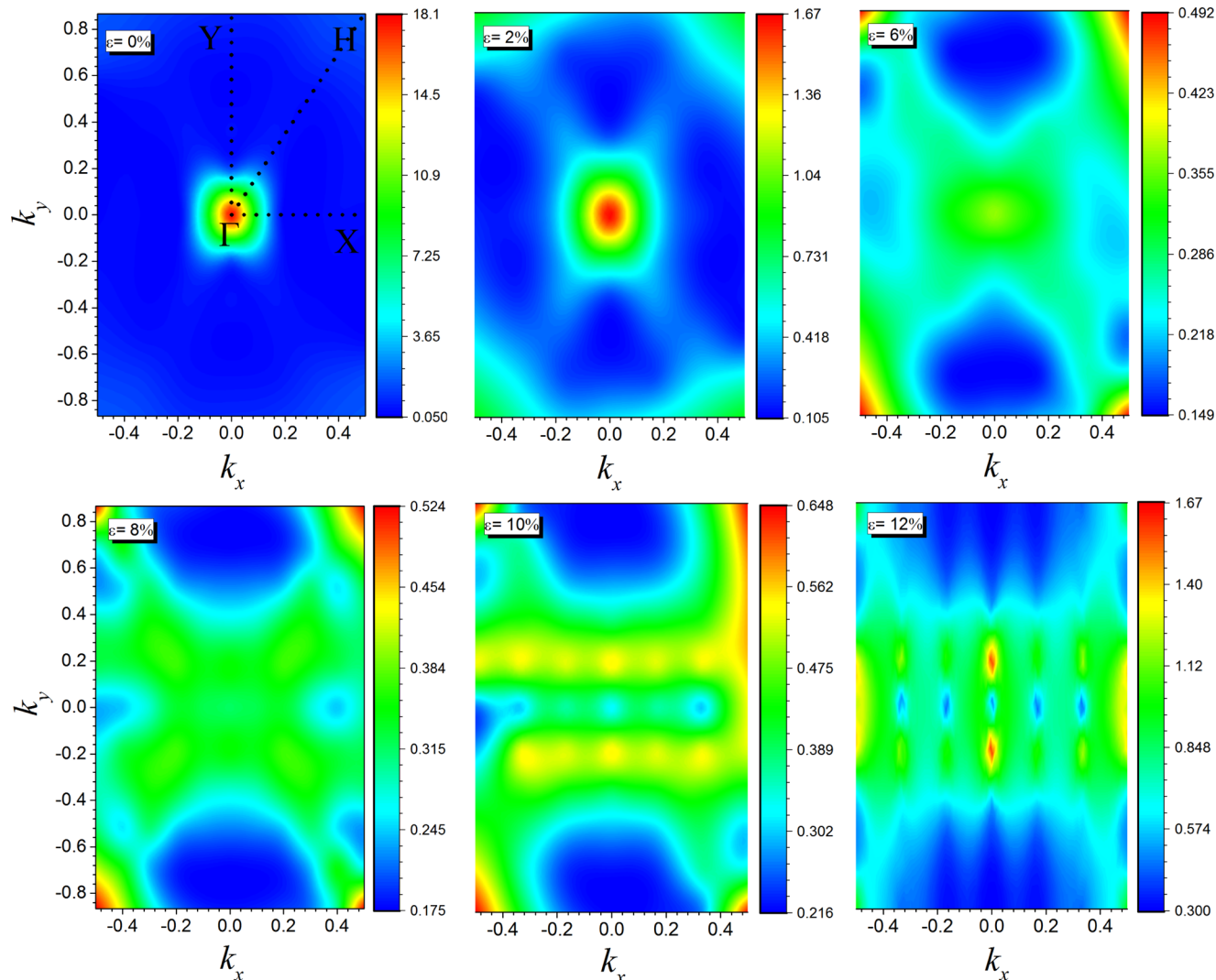


Figure 6. Distribution map of wave-vector-resolved EPC constants λ_q for the β_{12} borophene under different biaxial strains of 0, 2, 6, 8, 10, and 12%.

proportional to λ and $N(E_F)$ but inversely proportional to ω_{log} . λ is strongly related with $N(E_F)$. It indicates that the superconductivity in β_{12} borophene mainly depends on the DOS at FS under the strain. Our calculated λ and T_c under $4\% \leq \epsilon \leq 8\%$ approach to zero, which indicates the borophene loses its superconductivity although it is still a metal. The EPC in the β_{12} borophene is first suppressed and then enhanced under strain, which is different from that in the phosphorene and MoS₂.^{27,28} The T_c at $\epsilon = 12\%$ reaches 10.9 K with $\lambda = 0.69$, which is smaller than that of the pristine structure.

To illustrate clearly the EPC mechanism under different strains, the distribution map of wave-vector-resolved EPC constants λ_q has been shown in Figures 5 and 6. For the buckled triangle borophene, in general, the phonon frequency is softened by tensile strains and hardened by compressive strains. However, one can note that there is a dip in the lower acoustic phonon branch around the middle point between the Γ -X path (denoted as $1/2\Gamma X$ point), as circled in the red line in Figure 3a,b. When tensile or compressive strains are applied, lower phonon frequencies around the $1/2\Gamma X$ always become soft. As shown in Figure 5, λ_q changes a lot. The intensity of λ_q is increased with the increasing tensile strain and compressive strain. At $\epsilon = 0$, λ_q locates around the Γ point. And the intensity of λ_q around the Γ point makes up $\sim 85\%$ of the total

λ , whereas with the increasing tensile strain and compressive strain, λ_q at the Γ is gradually weakened, while λ_q around $1/2\Gamma X$ becomes stronger. When the strain is -2 or 3% , λ_q almost concentrates around the $1/2\Gamma X$ point. We can conclude that due to the lower acoustic phonon branch softened around the $1/2\Gamma X$ point undergoing the strain, the intensity of λ_q has a large enhancement and the focus of λ_q transforms from the Γ point to $1/2\Gamma X$ point gradually.

Figure 6 shows the distribution map of λ_q vs \mathbf{q} for the β_{12} borophene applied with the tensile strain. Calculations of the phonon dispersion suggest that the higher optical phonon branches move down but the lower acoustic phonon branches go upshift with increasing strain until $\epsilon = 10\%$. Because of the seriously destroyed B-B bonds, the imaginary frequency emerges between the Γ point and X point at the critical strains. Similar to that of the buckled triangle borophene, λ_q (more than 90%) at $\epsilon = 0\%$ mainly distributes around the Γ point. When applying a larger tensile strain, λ_q around the Γ point disappears abruptly and scatters averagely in the \mathbf{q} space and the intensity of λ_q becomes smaller. Under the strain larger than 10%, the intensity of λ_q begins to increase. The EPC strength is determined by the pair number of the electron at FS ($N(E_F)$) and lower acoustic phonon. Combining with the U-curve variation of $N(E_F)$, we can explain the variation of λ vs ϵ .

The Eliashberg spectral function is an important quantity in the calculation of T_c . Figure 7a,b shows $\alpha^2F(\omega)$ as a function

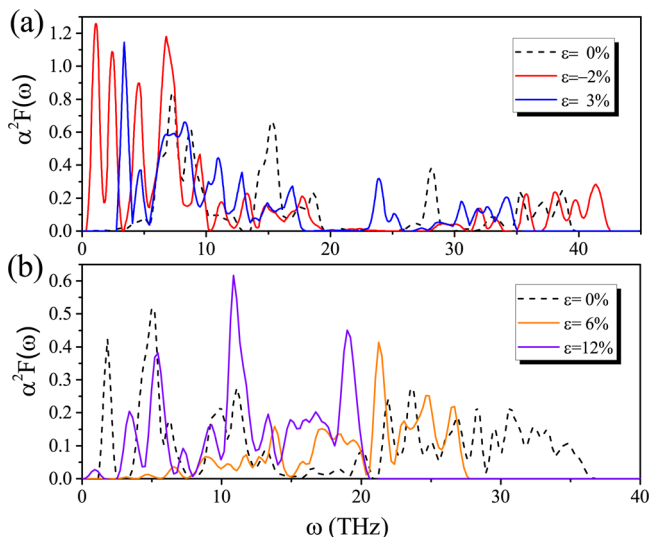


Figure 7. Eliashberg spectral function $\alpha^2F(\omega)$ as the function of ω . (a) $\alpha^2F(\omega)$ vs ω for the buckled triangle borophene under different biaxial strains of 0% (black dash line), -2% (red), and 3% (blue). (b) $\alpha^2F(\omega)$ vs ω for the β_{12} borophene under different biaxial strains of 0% (black dash line), 6% (orange), and 12% (purple).

of ω under different strains for the two types of borophenes, respectively. The whole profile of the Eliashberg spectral function moves to a lower-frequency region with increasing tensile strain, whereas it extends to a higher-frequency region under the compressive strain. The reason is that tensile strains soften the phonon spectrum and compressive strains stiffen it overall. The intensity of the Eliashberg spectral function is largely strengthened by both tensile and compressive strains in the buckled triangle borophene, whereas for the β_{12} borophene, it decreases with increasing tensile strain when it is lower than 6% but then it increases sharply. Moreover, the main peaks of $\alpha^2F(\omega)$ locate in the low-frequency range (0–10 THz) under critical strains of -2 and 3% in the buckled triangle borophene, which strongly enhances the EPC. In the

β_{13} borophene, the three main peaks of $\alpha^2F(\omega)$ gradually move from the low-frequency region (less than 10 THz) to the high-frequency region (larger than 20 THz) until the strain is 6% and then moves back to the middle-frequency region. Especially, at $\epsilon = 6\%$, the part of the Eliashberg spectral function with the frequency less than 10 THz, making the main contribution to the EPC under the pristine structure almost disappears. That may explain the loss of the superconductivity during $4\% \leq \epsilon \leq 8\%$. Compared with the pristine structure, although the total intensity of $\alpha^2F(\omega)$ has been enhanced at $\epsilon = 12\%$, the EPC constant λ and T_c decrease, the reason of which is that just only 1/3 part of $\alpha^2F(\omega)$ distributes in the low-frequency region, as can be seen in Figure 7b.

Because of the highly anisotropic structure of borophenes, we also considered the uniaxial strain effect on their superconductivity. The uniaxial strains along the a and b directions are applied on the buckled triangle borophene and β_{12} borophene. The variation of the superconducting transition temperature T_c , EPC constant λ , DOS of the FS $N(E_F)$, and logarithmically averaged phonon frequency ω_{\log} with the uniaxial strains are shown in Figure 8a,b, respectively. For the buckled triangle borophene, the structures are dynamically stable under $-2\% \leq \epsilon_a \leq 3\%$ and $-2\% \leq \epsilon_b \leq 8\%$. The largest ϵ_b (8%) in the buckled triangle borophene is much larger than that of the largest ϵ_a (3%), which can be explained by that the elastic modulus along the a direction is about 380 GPa nm, 2 times larger than that along the b direction.⁴² Contrast with the superconductivity of the buckled triangle borophene under the biaxial strains, the superconducting transition temperature and EPC constant decrease with the increase of the uniaxial strains along both directions, while the variation of the DOS of the FS and logarithmically averaged phonon frequency with ϵ_a and ϵ_b are anisotropic. The imaginary phonon modes will appear in the β_{12} borophene when the uniaxial strains are larger than 12% or less than -1%. Similar to the case under the biaxial strains, the T_c , λ , $N(E_F)$, and ω_{\log} vs ϵ_a or ϵ_b shares the same U-curve trend. The effects of the uniaxial strains ϵ_a and ϵ_b on the superconductivity show a good isotropy. Although the lattice of β_{12} borophene along the a and b directions exhibits different buckled configurations, the calculated mechanical properties reveal that the elastic modulus along the a and b directions

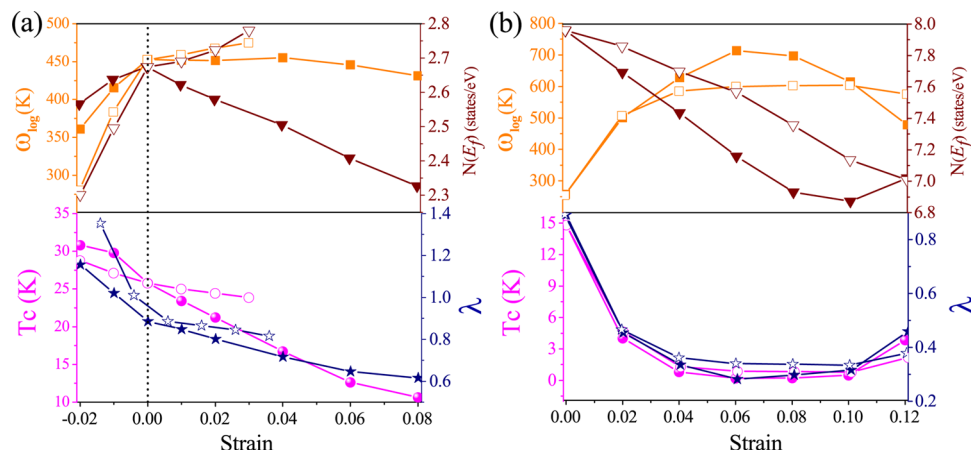


Figure 8. Superconducting transition temperature T_c (magenta), EPC constant λ (blue), DOS of the FS $N(E_F)$ (orange), and logarithmically averaged phonon frequency ω_{\log} (green) versus the uniaxial strains along the a (ϵ_a) and b (ϵ_b) directions for the (a) buckled triangle borophene and (b) β_{12} borophene, respectively. The curves marked with the hollow and solid symbols represent the uniaxial strain applied along the a and b directions, respectively.

(190 and 210 GPa nm) are close.⁴² The mechanisms of the uniaxial strain effect on the superconductivity of both borophenes also result from the stiffness or softening of the low-frequency acoustic phonon modes caused by the uniaxial strains.

CONCLUSIONS

In this work, we have systematically investigated the strain effects on the structure stability, EPC, and superconductivity of the buckled triangle and β_{12} borophene by first-principles calculations. In the pristine structures, we obtain the T_c of 25.8 K for the buckled triangle structure and 14.9 K for the β_{12} borophene. From the phonon dispersion spectra under different strains, we find that the buckled triangle borophene is stable under the strain region of $-2.0\% \leq \epsilon \leq 3.2\%$, whereas for the β_{12} borophene, either compressive strain or the strain beyond 12% gives rise to its instability. The electron density of states at FS, logarithmically averaged phonon frequency, EPC constant, and T_c vs the strain have been presented. The highest value of T_c reaches 32 K at $\epsilon = -1$ or 3%. Both tensile and compressive strains obviously enhance the EPC in the buckled triangle borophene, whereas the EPC of the β_{12} borophene first decreases when the tensile strain is lower than 6% and then increases until $\epsilon = 10\%$. Deep insight reveals that due to the lower acoustic phonon branch softened around the $1/2\Gamma X$ point undergoing the strain, the intensity of λ_q has a large enhancement and the focus of λ_q transforms from the Γ point to $1/2\Gamma X$ point gradually. Thus, T_c is increased except for $\epsilon = -2\%$ in the buckled triangle borophene. In spite of the large λ at $\epsilon = -2\%$, T_c decreases a lot because of the very small value of ω_{\log} . For the β_{12} borophene, the EPC constant and superconducting transition temperature show U-curve variations with the strain, which can be explained by the stiffness of the lower acoustic phonon branches and the U-curve variation of $N(E_F)$ mainly contributed by the p_z states. The distribution map of wave-vector-resolved EPC constants λ_q and the Eliashberg spectral function $\alpha^2 F(\omega)$ under different strains also suggests that the lower-frequency acoustic phonon affected by the strain plays an important role in the variation of the superconductivity. We also discussed the uniaxial strain effect on the superconductivity of borophenes and found that their effects along a and b directions are isotropic.

AUTHOR INFORMATION

Corresponding Author

*E-mail: junni@mail.tsinghua.edu.cn.

ORCID

Jun Ni: [0000-0001-9895-4248](https://orcid.org/0000-0001-9895-4248)

Notes

The authors declare no competing financial interest.

ACKNOWLEDGMENTS

This research was supported by the National Natural Science Foundation of China under Grants Nos. 11774195 and 11704322, the National Key Research and Development Program of China under Grants No. 2016YFB0700102, and the Natural Science Foundation of Shandong Province for Doctoral Program under Grant No. ZR2017BA017.

REFERENCES

- Bardeen, J.; Cooper, L. N.; Schrieffer, J. R. Theory of Superconductivity. *Phys. Rev.* **1957**, *108*, 1175–1204.
- Cudazzo, P.; Profeta, G.; Sanna, A.; Floris, A.; Continenza, A.; Massidda, S.; Gross, E. Ab Initio Description of High-Temperature Superconductivity in Dense Molecular Hydrogen. *Phys. Rev. Lett.* **2008**, *100*, No. 257001.
- McMahon, J. M.; Morales, M. A.; Pierleoni, C.; Ceperley, D. M. The Properties of Hydrogen and Helium under Extreme Conditions. *Rev. Mod. Phys.* **2012**, *84*, 1607–1653.
- Errea, I.; Calandra, M.; Pickard, C. J.; Nelson, J.; Needs, R. J.; Li, Y.; Liu, H.; Zhang, Y.; Ma, Y.; Mauri, F. High-Pressure Hydrogen Sulfide from First Principles: A Strongly Anharmonic Phonon-Mediated Superconductor. *Phys. Rev. Lett.* **2015**, *114*, No. 157004.
- Drozdov, A. P.; Eremets, M.; Troyan, I.; Ksenofontov, V.; Shylin, S. Conventional Superconductivity at 203 Kelvin at High Pressures in the Sulfur Hydride System. *Nature* **2015**, *525*, 73–76.
- Komelj, M.; Krakauer, H. Electron-Phonon Coupling and Exchange-Correlation Effects in Superconducting H_3S under High Pressure. *Phys. Rev. B* **2015**, *92*, No. 205125.
- Christensen, N. E.; Novikov, D. Predicted Superconductive Properties of Lithium under Pressure. *Phys. Rev. Lett.* **2001**, *86*, 1861–1864.
- Zhao, Y.; Zeng, S.; Ni, J. Superconductivity in Two-Dimensional Boron Allotropes. *Phys. Rev. B* **2016**, *93*, No. 014502.
- An, J. M.; Pickett, W. E. Superconductivity of MgB_2 : Covalent Bonds Driven Metallic. *Phys. Rev. Lett.* **2001**, *86*, 4366–4369.
- Kortus, J.; Mazin, I. I.; Belashchenko, K. D.; Antropov, V. P.; Boyer, L. L. Superconductivity of Metallic Boron in MgB_2 . *Phys. Rev. Lett.* **2001**, *86*, 4656–4659.
- Yildirim, T.; Güleren, O.; Lynn, J. W.; Brown, C. M.; Udovic, T. J.; Huang, Q.; Rogado, N.; Regan, K. A.; Hayward, M. A.; Slusky, J. S.; et al. Giant Anharmonicity and Nonlinear Electron-Phonon Coupling in MgB_2 : A Combined First-Principles Calculation and Neutron Scattering Study. *Phys. Rev. Lett.* **2001**, *87*, No. 037001.
- Eremets, M. I.; Struzhkin, V. V.; Mao, H.-k.; Hemley, R. J. Superconductivity in Boron. *Science* **2001**, *293*, 272–274.
- Mannix, A. J.; Zhou, X.-F.; Kiraly, B.; Wood, J. D.; Alducin, D.; Myers, B. D.; Liu, X.; Fisher, B. L.; Santiago, U.; Guest, J. R.; et al. Synthesis of Borophenes: Anisotropic, Two-Dimensional Boron Polymorphs. *Science* **2015**, *350*, 1513–1516.
- Feng, B.; Zhang, J.; Zhong, Q.; Li, W.; Li, S.; Li, H.; Cheng, P.; Meng, S.; Chen, L.; Wu, K. Experimental Realization of Two-Dimensional Boron Sheets. *Nat. Chem.* **2016**, *8*, 563–568.
- Tang, H.; Ismail-Beigi, S. Novel Precursors for Boron Nanotubes: The Competition of Two-Center and Three-Center Bonding in Boron Sheets. *Phys. Rev. Lett.* **2007**, *99*, No. 115501.
- Yang, X.; Ding, Y.; Ni, J. Ab Initio Prediction of Stable Boron Sheets and Boron Nanotubes: Structure, Stability, and Electronic Properties. *Phys. Rev. B* **2008**, *77*, No. 041402.
- Penev, E. S.; Bhowmick, S.; Sadrzadeh, A.; Yakobson, B. I. Polymorphism of Two-Dimensional Boron. *Nano Lett.* **2012**, *12*, 2441–2445.
- Yu, X.; Li, L.; Xu, X.-W.; Tang, C.-C. Prediction of Two-Dimensional Boron Sheets by Particle Swarm Optimization Algorithm. *J. Phys. Chem. C* **2012**, *116*, 20075–20079.
- Wu, X.; Dai, J.; Zhao, Y.; Zhuo, Z.; Yang, J.; Zeng, X. C. Two-Dimensional Boron Monolayer Sheets. *ACS Nano* **2012**, *6*, 7443–7453.
- Zhao, Y.; Zeng, S.; Ni, J. Phonon-Mediated Superconductivity in Borophenes. *Appl. Phys. Lett.* **2016**, *108*, No. 242601.
- Feng, B.; et al. Dirac Fermions in Borophene. *Phys. Rev. Lett.* **2017**, *118*, No. 096401.
- Delahaye, J.; Hassel, J.; Lindell, R.; Sillanpää, M.; Paalanen, M.; Seppä, H.; Hakonen, P. Low-Noise Current Amplifier Based on Mesoscopic Josephson Junction. *Science* **2003**, *299*, 1045–1048.
- De Franceschi, S.; Kouwenhoven, L.; Schönberger, C.; Wernsdorfer, W. Hybrid Superconductor–Quantum Dot Devices. *Nat. Nanotechnol.* **2010**, *5*, 703–711.
- Saira, O.-P.; Meschke, M.; Giazotto, F.; Savin, A. M.; Möttönen, M.; Pekola, J. P. Heat Transistor: Demonstration of

Gate-Controlled Electronic Refrigeration. *Phys. Rev. Lett.* **2007**, *99*, No. 027203.

(25) Savini, G.; Ferrari, A.; Giustino, F. First-Principles Prediction of Doped Graphane as a High-Temperature Electron-Phonon Superconductor. *Phys. Rev. Lett.* **2010**, *105*, No. 037002.

(26) Si, C.; Duan, W.; Liu, Z.; Liu, F. Electronic Strengthening of Graphene by Charge Doping. *Phys. Rev. Lett.* **2012**, *109*, No. 226802.

(27) Ge, Y.; Wan, W.; Yang, F.; Yao, Y. The Strain Effect on Superconductivity in Phosphorene: A First-Principles Prediction. *New J. Phys.* **2015**, *17*, No. 035008.

(28) Zeng, S.; Zhao, Y.; Li, G.; Ni, J. Strongly Enhanced Superconductivity in Doped Monolayer MoS₂ by Strain. *Phys. Rev. B* **2016**, *94*, No. 024501.

(29) Gao, M.; Li, Q.-Z.; Yan, X.-W.; Wang, J. Prediction of Phonon-Mediated Superconductivity in Borophene. *Phys. Rev. B* **2017**, *95*, No. 024505.

(30) Penev, E. S.; Kutana, A.; Yakobson, B. I. Can Two-Dimensional Boron Superconduct? *Nano Lett.* **2016**, *16*, 2522–2526.

(31) Baroni, S.; de Gironcoli, S.; Dal Corso, A.; Giannozzi, P. Phonons and Related Crystal Properties from Density-Functional Perturbation Theory. *Rev. Mod. Phys.* **2001**, *73*, 515–562.

(32) Giannozzi, P.; Baroni, S.; Bonini, N.; Calandra, M.; Car, R.; Cavazzoni, C.; Ceresoli, D.; Chiarotti, D. L.; Cococcioni, M.; Dabo, I.; et al. QUANTUM ESPRESSO: A Modular and Open-Source Software Project for Quantum Simulations of Materials. *J. Phys.: Condens. Matter* **2009**, *21*, No. 395502.

(33) Perdew, J. P.; Chevary, J. A.; Vosko, S. H.; Jackson, K. A.; Pederson, M. R.; Singh, D. J.; Fiolhais, C. Atoms, Molecules, Solids, and Surfaces: Applications of the Generalized Gradient Approximation for Exchange and Correlation. *Phys. Rev. B* **1992**, *46*, 6671–6687.

(34) McMillan, W. L. Transition Temperature of Strong-Coupled Superconductors. *Phys. Rev.* **1968**, *167*, 331–344.

(35) Allen, P. B.; Dynes, R. C. Transition Temperature of Strong-Coupled Superconductors Reanalyzed. *Phys. Rev. B* **1975**, *12*, 905–922.

(36) Eliashberg, G. Interactions Between Electrons and Lattice Vibrations in a Superconductor. *J. Exp. Theor. Phys.* **1960**, *11*, 696–702.

(37) Xiao, R.; Shao, D.; Lu, W.; Lv, H.; Li, J.; Sun, Y. Enhanced Superconductivity by Strain and Carrier-Doping in Borophene: A First Principles Prediction. *Appl. Phys. Lett.* **2016**, *109*, No. 122604.

(38) Richardson, C.; Ashcroft, N. High Temperature Superconductivity in Metallic Hydrogen: Electron-Electron Enhancements. *Phys. Rev. Lett.* **1997**, *78*, 118–121.

(39) Lee, K.-H.; Chang, K.; Cohen, M. L. First-Principles Calculations of the Coulomb Pseudopotential μ^* : Application to Al. *Phys. Rev. B* **1995**, *52*, 1425–1428.

(40) Cheng, C.; Sun, J.-T.; Liu, M.; Chen, X.-R.; Meng, S. Tunable Electron-Phonon Coupling Superconductivity in Platinum Diselenide. *Phys. Rev. Mater.* **2017**, *1*, No. 074804.

(41) Huang, L.-F.; Gong, P.-L.; Zeng, Z. Phonon Properties, Thermal Expansion, and Thermomechanics of Silicene and Germanene. *Phys. Rev. B* **2015**, *91*, No. 205433.

(42) Mortazavi, B.; Rahaman, O.; Dianat, A.; Rabczuk, T. Mechanical Responses of Borophene Sheets: A First-Principles Study. *Phys. Chem. Chem. Phys.* **2016**, *18*, 27405–27413.